NRIAG Journal of Astronomy and Geophysics 7 (2018) 237–246

Contents lists available at ScienceDirect

NRIAG Journal of Astronomy and Geophysics

journal homepage: www.elsevier.com/locate/nrjag

Full length article

Co-seismic ionospheric GPS-TEC disturbances from different source characteristic earthquakes in the Himalaya and the adjoining regions

Param K. Gautam*, Vishal Chauhan, Rajesh Sathyaseelan, Naresh Kumar, John P. Pappachen

Wadia Institute of Himalayan Geology, Dehradun, Uttarakhand, India

ARTICLE INFO

Keywords:
GPS
Co-seismic
Ionospheric TEC
Earthquake
Himalaya

ABSTRACT

Co-seismic ionospheric disturbances (CIDs) due to different source characteristic earthquakes are investigated through GPS-derived vertical total electron content (VTEC). We investigated VTEC changes related with Moderate, Strong, Major and Great earthquakes occurred at different tectonic settings in both Himalaya and non-Himalayan regions. The VTEC and its anomalies are computed using GPS data obtained from the local network of GPS stations in Himalaya with the IGS stations surrounding the epicentre region. Irrespective of the source characteristics, significant CIDs are observed during Major and Great earthquakes, namely; (i) the Mw 7.8, 25th April 2015 Gorkha earthquake, (ii) the Mw 7.6, 8th October 2005 Kashmir earthquake, and (iii) the Mw 8.6, 28th March 2005 Nias–Simeulue earthquake.

The VTEC anomalies due to the Gorkha event are observed 21.15 min after the earthquake origin time and continued till 22.78 min with the amplitude range from −0.530 to 0.517 (± 0.11) TECU. CIDs associated with the Kashmir earthquake are noticed only at two GPS sites (NADI and PAN2) roughly after 23 min of the earthquake occurrence. But, it continued around 14 min with the amplitude range from −0.12 to 0.177 TECU (± 0.02 TECU = 1σ). However, for the case of Ocean-Island Arc Nias–Simeulue earthquake, anomalous CIDs were observed only at GPS site NTUS, where the disturbances started around 25.58 min later and continued around 17.92 min with amplitude range from −0.077 to 0.058 TECU (± 0.02 TECU = 1σ). We inferred that the CIDs originated because of earthquakes in Himalaya have relatively larger VTEC magnitudes (> 15 TECU) that propagates faster in reaching and registering in the ionospheric layers compared with the non-Himalayan earthquakes. Secondly, different lithospheric-ionospheric coupling mechanism is operating in transferring the seismic energy, which originated from the Continent-Continent and the Tsunami genic Ocean-Island Arc collision zone, to the ionosphere.

1. Introduction

Ionospheric layer exists in the Thermosphere part of the upper atmosphere which contains free electrons and positively charged ions. The maximum ionization takes place at a height of about 350–400 km and ionospheric electrons are free to move in the presence of ambient electric and magnetic fields. Earthquake is a well-known source for the atmospheric and ionospheric perturbations. In addition volcanic eruptions, nuclear and chemical explosions (Row, 1967), rocket and space shuttle launching (Ding et al., 2014; Calais and Minster, 1996), ballistic missiles (Ozeki and Heki, 2010), asteroids and even surface mine blasts, generate significant ionospheric perturbations (Calais and Minster, 1996). Solar events (coronal mass ejections and solar flares), atmospheric phenomena (thunderstorms and lightning), and meteorological events (typhoons and tornadoes) (Huang et al., 1985; Bishop et al., 2006) may also cause ionospheric perturbations. CIDs are quite interesting phenomena that involve coupling of lithosphere, atmosphere and ionosphere, which inspired many researchers around the globe (Liperovsky et al., 1992; Parrot et al., 1993; Gaivoronskaya and Pulinets, 2002; Pulinets et al., 2003; Pulinets, 2004). In the present work we analyzed GPS-based TEC data to study the behaviour of ionosphere as well as its co-seismic disturbances.

GPS transmits signals at two different frequencies L_1 (1575.42 MHz) and L_2 (1227.60 MHz), which is useful for ionospheric correction for the precise positional measurements. The ionospheric delay is a function of TEC along the signal path and the frequency. This delay can be minimized through a linear combination L_1 and L_2 GPS Carrier signals. The columnar distribution of number of charged particles or TEC values expressed in TECU (1 TECU = 10^{16} electrons m^{-2}) between the ground antenna and the satellite at higher altitudes from 250 to 400 km can be

Peer review under responsibility of National Research Institute of Astronomy and Geophysics.
* Corresponding author at: Wadia Institute of Himalayan Geology, 33, G. M. S. Road, Dehradun 248001, Uttarakhand, India.
E-mail address: param@wihg.res.in (P.K. Gautam).

https://doi.org/10.1016/j.nrjag.2018.05.009
Received 13 June 2017; Received in revised form 25 May 2018; Accepted 26 May 2018
Available online 07 June 2018

Table 1
Location, timing, epicentre and hypocentres of earthquakes used in this study.

S.N.	JD	Date	Time (UTC)	Lat. (°N)	Long.(°E)	Depth (km)	Mag. (M_w)	Region
1	87	28.03.1999	19:05:14	30.4	79.4	21	6.8	Chamoli
2	361	26.12.2004	00:58:52.5	3.4	95.9	26.1	9.0	Sumatra
3	87	28.03.2005	16:09:35.29	2.1	97.1	30	8.1	Sumatra
4	281	08.10.2005	03:50:40	34.5	73.6	7.9	7.3	Kashmir
5	203	22.07.2007	23:02:13	31.2	78.2	33	5.0	Kharsali
6	261	18.09.2011	12:40:49.58	27.8	88.1	29.6	6.9	Sikkim
7	115	25.04.2015	06:11:25	28.1	84.6	10	7.9	Nepal
8	299	26.10.2015	09:09:33.75	36.4	70.8	231.1	7.6	Hindukush
9	3	03.01.2016	23:05:16	24.8	93.5	17	6.7	Manipur

estimated, from the observed near- and far-field slant GPS signals followed by large earthquakes (Trigunait et al., 2004). Such earthquakes can be studied using GPS derived vertical TEC (VTEC), and its variations less than 0.01 TECU can be measured. But for Moderate earthquakes of magnitudes Mw from 5 to 5.9, the perturbations tend to become small (Ducic et al., 2003). It has been shown in the previous studies that dense GPS arrays can provide an opportunity to investigate ionospheric perturbations in the most efficient manner (Reddy, 2016; Reddy and Seemala, 2015; Seemala and Valladares, 2011; Ogawa et al., 2012; Sunil et al., 2015; Cahyadi and Heki, 2013, 2015). Some advanced techniques, such as HF Doppler sounding (Artru et al., 2004; Ogawa et al., 2012), DEMETER (Ryu et al., 2014), Over-The-Horizon Radar (Occhipinti et al., 2010), Faraday rotation measurements using linearly polarized electromagnetic signals from geostationary satellites (Davies, 1980), and GPS (Ducic et al., 2003; Heki, 2011; Saito et al., 2011) have also shown that ionospheric plasma perturbations can be generated by large earthquakes. Study of seismo-ionospheric response of earthquakes from 1965 to 2013, have shown that only earthquakes of Mw ≥ 6.5 generate significant wave response in the ionosphere (Perevalova et al. 2014). Astafyeva et al. (2011) has first reported that TEC is higher for earthquakes of larger magnitudes and also demonstrated that shallow earthquakes with magnitude Mw 7.2–7.8 cause co-seismic perturbations with near-field amplitude of 0.2–0.4 TECU (lasting 4–8 min). While, Great earthquakes of ~Mw 9.0 and above produce extremely large perturbations of ~1–3 TECU (lasting 30–40 min). The focal mechanism solutions, which represent the sub-surface dynamics of earthquake source characteristics also play a significant role in manifesting ionospheric response (Astafyeva and Heki, 2009). Cahyadi and Heki (2015) explained the relation between induced TEC and the moment magnitude of an earthquake. Studies on earthquake propagation dynamics (Liu et al., 2006, 2011) had revealed invoking of three different types of co-seismic perturbations in the ionosphere caused by the propagating surface Rayleigh waves; which are (1) the co-seismic crustal displacements, (2) by tsunamis and (3) post-seismic, four minute duration mono-periodic atmospheric resonances (Liu et al., 2011; Rolland et al., 2011a, 2011b). Recently, TEC based studies on the response of three largest submarine earthquakes in Japan, Chile, and Indonesia; Kakinami et al. (2012) reported, an initiation of sudden depletion of the ionospheric total electron content (TEC) that consequently followed by a sudden co-seismic TEC enhancement, which lasted for a few tens of minutes. This phenomena was observed just above the tsunami source area, where the ionospheric depletion was attributed “to the down welling of the sea surface” as a result of tsunami generation. Kakinami et al. (2012) also emphasized that inland earthquakes do not produce the ionospheric electron hole.

The Himalayan mountain chain is developed as a result of ongoing collision between India and the Eurasian tectonic plates, which was started more than 60 million years ago. The continuing collision has formed Himalayan inter-plate zone causing the development of many Faults, Folds, Windows, Nappe etc., (Gansser, 1964). Geological, geodetic and seismic studies on the slip rates of Faults in Asia show that approximately one-third of the present-day convergence rate between India and the Asia ($58 \pm 4\,mm\,yr^{-1}$) is responsible for the shortening, uplift and moderate seismicity of the Himalaya (Bilham et al., 1997). Strong magnitude earthquakes sporadically occur in Himalaya along the main seismic belt owing to the ongoing continent-continent collision and crustal under thrusting. Thus the source characterization of seismicity in this region is mainly the Thrust mechanism with very minor influence of strike-slip type crustal movement. Such a continent-continent collision zone tectonics, (as the case for recent Nepal earthquakes) provides ample opportunity to understand and compare how the TEC variations are influenced by tectonic collision with respect to an oceanic collisional zone (as for the case of Sumatra earthquakes). With that objective, we studied nine earthquakes of different magnitudes ($> M_w$ 6) occurred at different tectonic settings in the Himalaya and Sumatra regions for analysing co-seismic ionospheric TEC responses. Details of events considered in this study are shown in Table 1 with their locations mentioned in Fig. 1 in the seismo-topographic map. The data analysis consists of GPS Rinex observations along with the IGS ephemeris files from the local Himalayan permanent GPS stations as well as from the IGS GPS network -as shown as different coloured triangles in Fig. 1- around the considered earthquake epicentres. Details of station locations considered for significant earthquakes from Nepal, Kashmir and Sumatra regions are given in Tables 2, 3 and 4 with pictorial representation in Fig. 1.

2. Seismic events

GPS data recorded during the time of occurrence of 9 regional and distant seismic events, shown as yellow stars in Fig. 1, are analyzed. Among that, eight events are having Magnitudes more than 6.5; except the 22nd July 2007 Kharshali earthquake, which is a Moderate magnitude event. Details of the earthquake source parameters along with their region of occurrences are given in Table 1. Focal mechanism solutions of eight events were extracted from the CMT catalogue of USGS (Dziewonski et al., 1981; Ekström et al., 2012) and the remaining Mw 5.0 Kharshali earthquake was taken from Kumar et al., 2012a and as shown as beach ball in Fig. 1. From Table 1, it is evident that five earthquakes are from the Himalayan region including the recent devastating Mw 7.8 Gorkha earthquake of 2015 and the Mw 7.6 major Kashmir earthquake of 2005. These earthquakes are shallow focused within the upper crust and importantly four such events have their hypocentres close to the sub-surface tectonic boundary called the Main Himalayan Thrust (MHT), along which the under-thrusting Indian Plate detached from the Himalayan wedge and the Eurasian Plate. Focal mechanism solutions of these four earthquakes suggest thrust/reverse mechanisms and indicating thrusting nature of the Indian plate beneath the Eurasian plate along the detachment zone. Similarly, the Sikkim earthquake of 2011 was a deeper event occurred at a depth of ~47 km (Arora et al., 2014). Source mechanism of this event was strike slip, which is an exception in a thrusting regime. However, it was originated in the deeper part of the crust and guided by transverse lineament as per the prevailing tectonic deformation exist at that part of the Himalaya. Another recent earthquake of 2015 was from the Hindukush

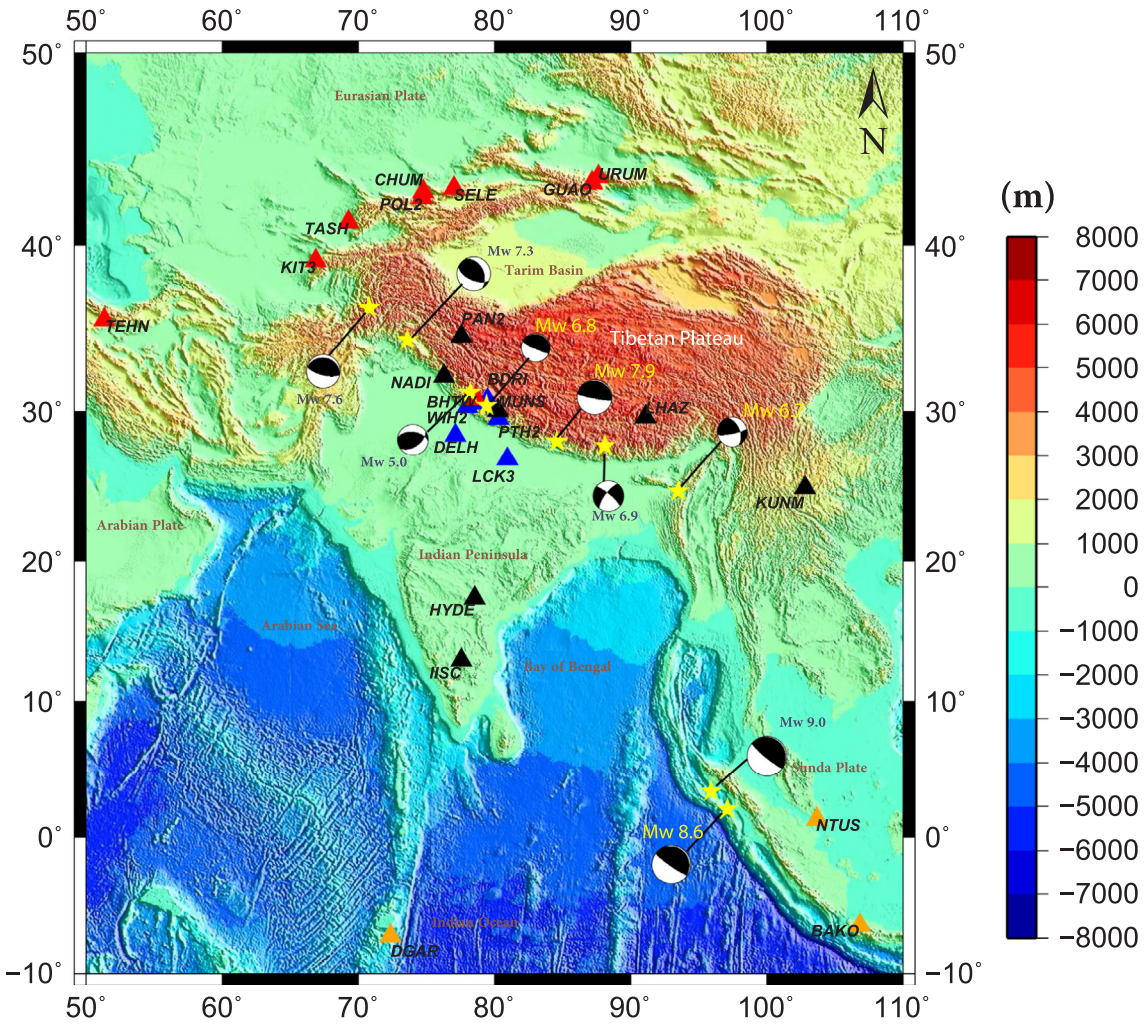

Fig. 1. Regional Topography and Bathymetry of the study area (Source: GEBCO); Yellow stars represent the epicentres of nine major earthquakes considered in this study. GPS station locations as colour filled triangles: - Blue for Nepal earthquake; Red for Kashmir earthquake; Orange for Sumatra earthquake and Black for common stations for all the three events. Fault Plane Solutions are from the CMT solution catalogue. (For interpretation of the references to colour in this figure legend, the reader is referred to the web version of this article.)

Table 2
GPS stations with their epicentre distances used for the analysis of 2015 Nepal earthquake.

Station code	Lat. (°N)	Long.(°E)	Epicentral distance (km)	Azimuth angle (°)
bdri	30.74	79.49	575.20	301.95
delh	28.48	77.12	732.88	275.09
ghut	30.53	78.74	628.40	296.88
lck3	26.91	80.95	382.90	250.67
lhaz	29.65	91.10	656.40	73.14
pth2	30.32	78.01	685.43	292.77
wih2	29.57	80.28	451.05	292.32

Table 3
GPS stations with their epicentre distances used for the analysis of 2015 Kashmir earthquake.

Station code	Lat. (°N)	Long. (°E)	Epicentral distance (km)	Azimuth angle (°)
bhtw	30.82	78.61	621.29	130.13
chum	42.99	74.75	947.20	5.49
guao	43.47	87.17	1532.17	45.49
hyde	17.41	78.55	1963.70	164.38
iisc	13.02	77.57	2423.61	169.63
kit3	39.13	66.88	789.68	312.44
kunm	25.02	102.79	2992.41	102.74
lhaz	29.65	91.10	1729.15	103.40
muns	30.06	80.24	794.15	126.85
nadi	32.24	76.30	354.03	134.89
pan2	34.71	77.57	360.69	85.58
pol2	42.67	74.69	911.48	5.44
sele	43.17	77.01	1005.57	15.85
tash	41.32	69.29	846.82	334.58
tehn	35.69	51.33	2028.82	280.10
urum	43.78	87.63	1582.39	45.23
wuhn	30.53	114.35	3817.43	85.06

region; a deeper event of intermediate focus depth of 230 km. In fact, in the Hindukush, and the adjoining north western region of the Himalaya, the predominance of intermediate focused earthquakes is related with the delaminated part of the subducting Indian plate. This earthquake also shown pure thrust mechanism.

Apart from this, we have also analyzed GPS derived TEC data during the time of occurrence of devastating Great Sumatra earthquake (Mw 9.2) of 26th December 2004 that caused havoc in the subcontinent (Banerjee et al., 2005) and recorded as the strongest and first Tsunamigenic event in the history of instrumental seismology. Besides, a

Table 4
GPS stations with their epicentre distances used for the analysis of 2015 Sumatra earthquake.

Station code	Lat. (°N)	Long. (°E)	Epicentral distance (km)	Azimuth angle (°)
bako	−6.49	106.84	1442.16	131.52
coco	−12.18	96.83	1588.69	181.10
dgar	−7.26	72.37	2936.24	248.99
hyde	17.41	78.55	2648.04	311.21
iisc	13.02	77.57	2469.92	300.44
kunm	25.02	102.79	2621.83	12.96
lhaz	29.65	91.10	3129.71	348.88
muns	30.06	80.24	3582.68	331.89
nadi	32.24	76.30	3996.86	329.21
ntus	1.34	103.67	734.62	96.41
pan2	34.71	77.57	4152.35	333.05
wuhn	30.53	114.35	3646.04	28.13

subsequent Great Magnitude (Mw 8.6) event, called the 2005 Nias-Simeulue earthquake occurred four months later from the same source characteristic region of Ocean-Island Arc collision zone was also analyzed. Both these earthquakes have predominantly thrust mechanism under which the oceanic lithosphere of the Indian plate got subducted below the overriding Sumatra plate in the south-eastern part of the Indian Ocean region. This region is highly vulnerable and many Major or Strong Magnitude earthquakes are occurring due to the ongoing viscoelastic relaxation phase of the asthenospheric mantle (Pollitz et al., 2006) and subsequent crustal stress changes in the subducting oceanic lithospheric slab. As a result shallow focused seismic events are also observed in this source region. We also considered a shallow focused strike slip event of Mw 6.7 (Kumar et al., 2016) that occurred recently in the Manipur region, where the present day active continent-continent subduction takes place due to the eastward movement of the India Plate beneath the Burma Plate along the Indo-Burmese subduction Arc. All these mentioned events are important earthquakes of the subcontinent and the present work has a merit of analysis during their occurrence. Thus in this study, we have analyzed GPS derived TEC data from mainly three different source characteristics, such as (1) Continent-Continent collision zone in the Himalayan region with predominantly Thrust mechanism (2) Ocean-Island Arc collisional zone in the Sumatra Andaman with Thrust mechanism and (3) Continent-Continent collision zone along the present day active Indo-Burmese subduction Arc, where the strike-slip mechanism is regulating the subduction tectonics.

3. Methodology and data analysis

The surface Rayleigh waves, that generated and radiated out from the epicentre of a large Magnitude earthquake cause surface displacements. This sudden impulsive displacement of the ground surface generates atmospheric pressure waves that propagate upward at infrasonic speed into the atmosphere, which interacts with the ionosphere at height of ~400 km within 10 min's and produces an N shaped waveform disturbances (Astafyeva et al., 2013). Earthquakes having Magnitude more than 6.5 with epicentre distance of Ionospheric Piercing Point (IPP) within 1000 km reflect a significant wave response in the ionosphere (Perevalova et al., 2014; Otsuka et al., 2006; Tsugawa et al., 2011). In the aftermath of an earthquake the propagating lower atmospheric disturbances may change the ionospheric electron density through the energy coupling of atmospheric infrasonic pressure waves to the ionospheric gravity waves. The spatio-temporal variation of TEC anomalies are of the order of tens of metres to hundreds of kilometres and may happen within a few minutes to hours.

TEC from GPS measurements provide better spatial and temporal coverage as it was explained by Hofmann-Wellenhof et al., 2001 and Hocke and Pavelyev, 2001. The propagation of GPS signals L1 (1575.42 MHz) and L2 (1227.6 MHz) through ionosphere cause group delay and phase advances as ionosphere is a dispersive medium. The delay and phase advancement of the signal depend upon the integrated columnar electron density or TEC which has been obtained by considering a spherical shell ionosphere. The GPS technology enables to estimate the integrated TEC $I_0(t)$ or Slant TEC (STEC) variations along the satellite-receiver path on the basis of TEC phase measurements

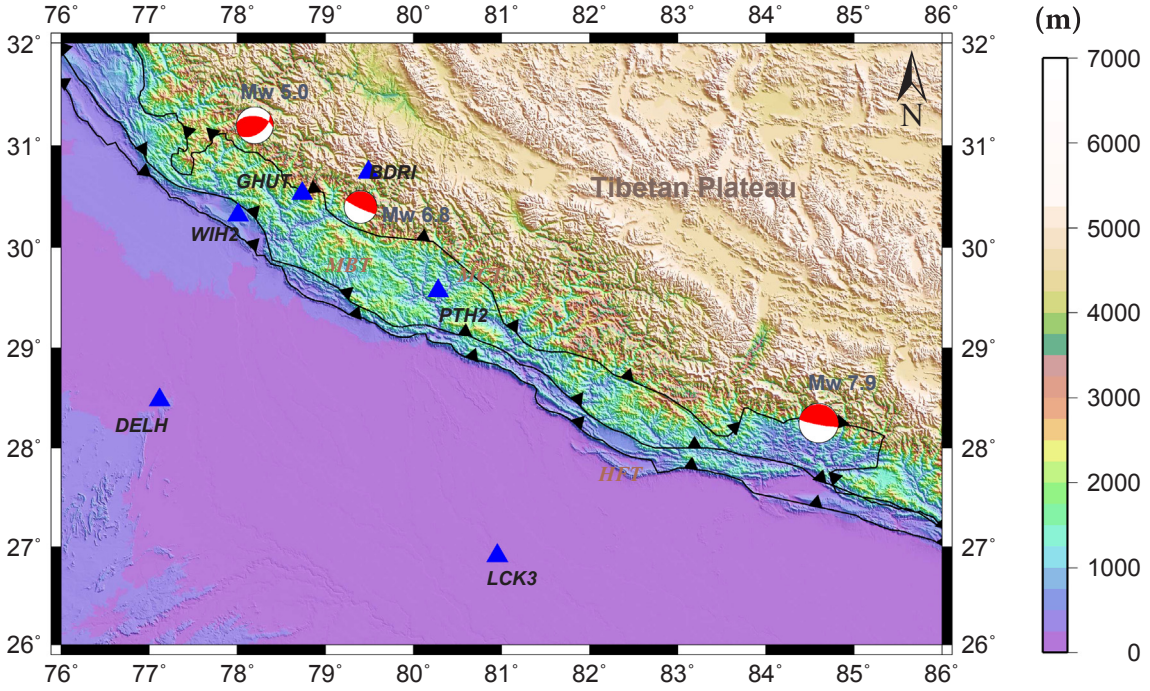

Fig. 2. . Regional topography (Source: GTOPO 30) and major thrust structures in an around the Nepal earthquake region. Beach ball represents the fault plane solutions of three major earthquakes occurred earlier in this area. Blue triangles represent the locations of GPS stations considered in this case. (For interpretation of the references to colour in this figure legend, the reader is referred to the web version of this article.)

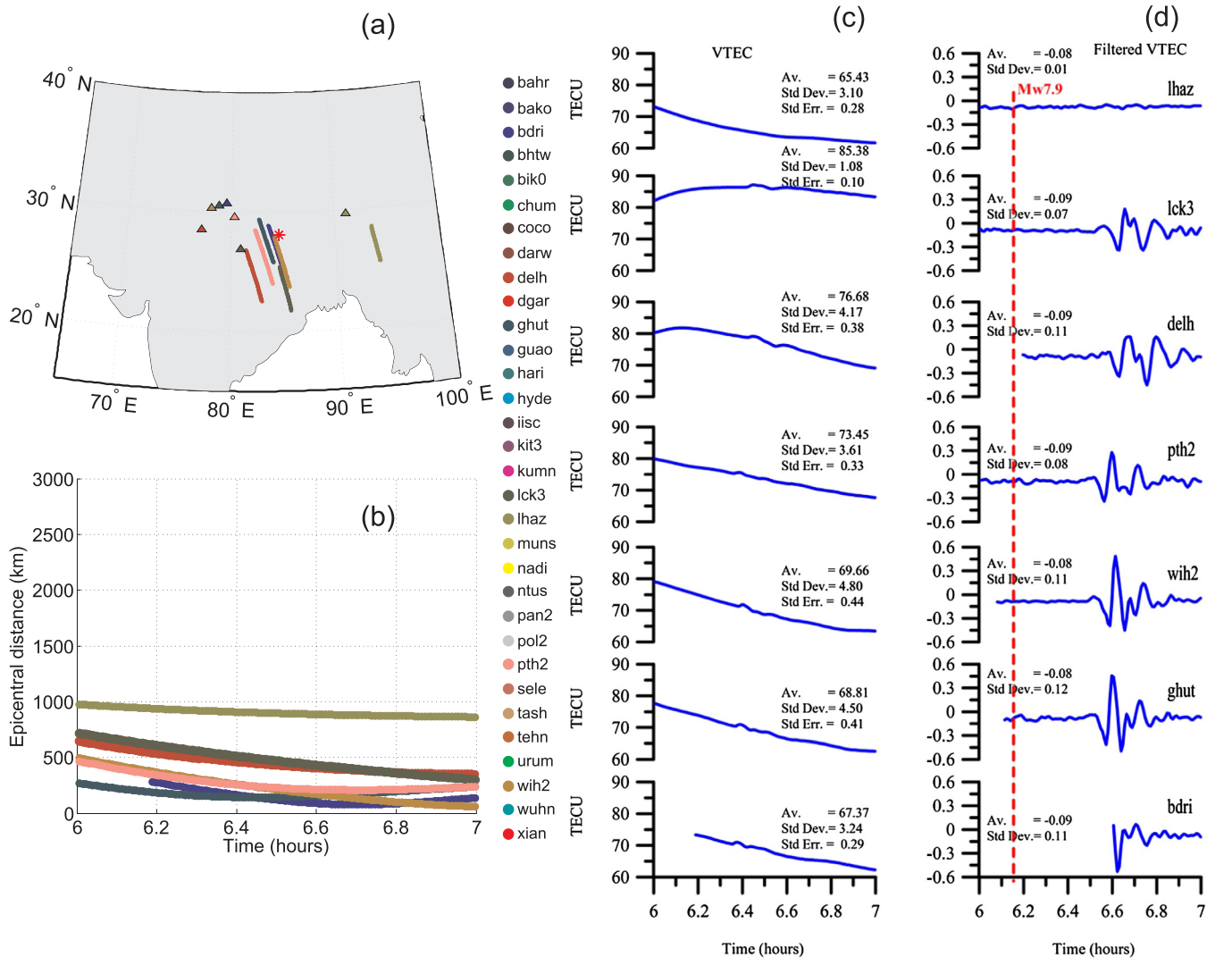

Fig. 3(i). . For locked satellite PRN-27 for the Nepal 2015 earthquake: - (a) IPP plots at stations given in Table 2. (b) Epicentral distances of Ionospheric Piercing Point (IPPs) Vs time plots at stations given in Table 2. (c) Estimated Co-seismic ionospheric VTEC at each stations. (d) Band pass filtered Co-seismic ionospheric VTEC anomalies at each station.

made with each of the spatially separated two-frequency GPS receivers using the formula (Calais and Minster, 1996; Afraimovich et al., 2001):

$$I_0(t) = \frac{1}{40.308}\frac{f_1^2 f_2^2}{f_1^2 - f_2^2}[(L_1\lambda_1 - L_2\lambda_2) + const + nL]$$

where L1 and L2 represent the carrier phase measurements and f_1 and f_2 are their respective frequencies; λ_1 and λ_2 are the corresponding wavelengths. $L_1\lambda_1$ and $L_2\lambda_2$ are the increments of the radio signal phase path caused by the phase delay in the ionosphere; 'const' is some unknown initial phase path caused by the unknown number of total phase rotations along the line of sight and 'nL' is the error in determining the phase path. Computation of vertical TEC (VTEC) from the instantaneous 'STEC' is as explained by Klobuchar, (1986) and Rama Rao et al. (2006) using the satellite elevation angle 'θ' and the receiver and satellite biases. Here, the instantaneous 'STEC' values are multiplied with the slant factor to get the vertical TEC, such as VTEC = TEC * h/L; where 'h' is the mean ionospheric thickness of around 1100 km and 'L' is the length of the ray path through the ionosphere. Variations of the regular ionosphere, and also trends introduced by the motion of the satellite are eliminated using the procedure of removing the trend defined as a polynomial of the third order on a given temporary interval.

In this study, continuously operating reference station (CORS) GPS data in the Rinex format acquired at every 30 sec interval from different IGS sites (ftp://cddis.gsfc.nasa.gov) along with our data from WIHG CORS network in an around the study area have been used for the TEC computation. We adopted the source code as developed in the works of Rama Rao et al. (2006), and Kumar et al., 2012b to study the GPS-TEC variations in the Indian region. Along with Rinex observation files we also obtained BRDC Navigation files (ftp://ciddis.gsfc.nasa.gov/gps/data/) and Differential Code Bias (DCB) data (http://www.aiub.unibe.ch/download/CODE) as inputs for the Ionospheric TEC calculations. The program reads Rinex observation files and calculate phase and group from L1, L2, P1, and P2 and these carrier phases and Group delay measurements are used for the calculation of Slant TEC (STEC) by applying receiver, satellite and inter-channel bias corrections. Then the Vertical TEC (VTEC) at Ionospheric piercing point are calculated from STEC using a mapping function as explained earlier by applying elevation (only $> 30^\circ$ are considered) and azimuth angles of the satellite with respect to the station, from ephemeris at the given time.

The seismo-ionospheric disturbances are computed for the earthquakes mentioned in Table 1 and also shown in Fig. 1. Tables 2, 3 and 4 show GPS station locations and their epicentral distances with azimuths for those earthquakes occurred in Nepal, Kashmir and Sumatra regions, respectively. Data from GPS stations used for these three major events are also marked as different coloured triangles in Fig. 1; such that, data

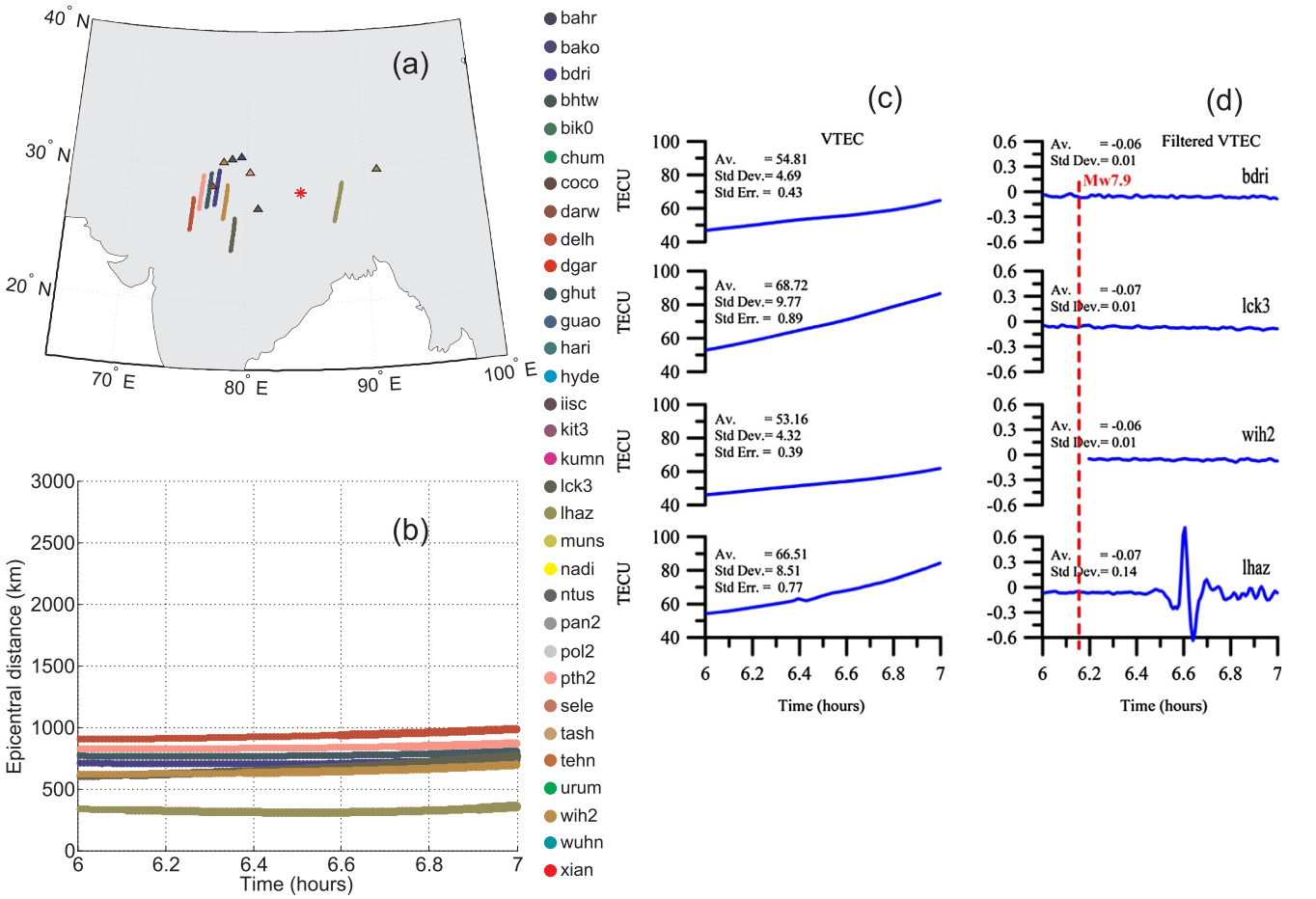

Fig. 3(ii). . For locked satellite PRN-3 for the Nepal 2015 earthquake: - (a) IPP plots at stations given in Table 2. (b) Epicentral distances of Ionospheric Piercing Point (IPPs) Vs time plots at stations given in Table 2. (c) Estimated Co-seismic ionospheric VTEC at each stations (d) Band pass filtered Co-seismic ionospheric VTEC anomalies at each station.

from black triangle stations are common for all the three events. While blue, red and orange coloured triangles are stations used for the cases of Nepal, Kashmir and Sumatra events respectively. We analyzed the GPS data on the day of each earthquake based on 1) the availability of satellites PRN'S shown as IPP Fig. 2) at various distances from the epicentral point to the sub-ionospheric piercing points and shown in the epicentral-time plot and 3) the respective computed vertical TEC values and their band pass (2–10 mHz) filtered VTEC anomalies during each earthquake at various stations given in their respective tables. The computed vertical TEC values for the event day has been analyzed for a duration of an hour after subjecting it to band pass filtering and subsequently correlated with the earthquake events.

4. Results and discussion

In this study, we analyzed GPS based Ionospheric TEC variation associated with earthquakes of different source characteristics - as explained in Table 1- with their source mechanisms shown in Fig. 1. We have considered total nine events, out of which three significant events originated from two different tectonic regimes in and around the Indian Plate show CIDs. These events are, (1) in the continent-continent Himalayan collision zone, the occurrence of 25th April 2015, Mw 7.8 Gorkha earthquake and the 8th October 2005, Mw 7.6 Kashmir earthquake; and (2) the 28th March 2005 Great Magnitude (Mw 8.6) Nias-Simeulue earthquake occurred at the Ocean-Island Arc collisional boundary in the West coast of the Northern Sumatra. The observations on CIDs of these earthquakes are explained below.

(i) The Gorkha Mw 7.9 earthquake of 25th April 2015

The Gorkha earthquake of magnitude Mw 7.9 occurred on 25th April 2015 (latitude 28.147°N, longitude 84.708°W; depth ~15 km; 06:11:26 UTC), at ~34 km away from Lamjung District (Avouac et al., 2015). The seismic source characteristics and focal mechanism of the earthquake are shown in Fig. 2, which suggest that it was caused by a slip along the sub-surface Main Himalayan Thrust that separates the overriding Himalayan wedge from the under thrusting Indian Plate. The epicentre location of this event is denoted in Fig. 2 and seen just north of the major plate boundary fault called the Main Central Thrust (MCT), which separates the Higher Himalayan crystalline rocks at its north from the south bound Lesser Himalayan Metamorphic rocks. CIDs due to this Major earthquake have been studied using data from seven GPS stations and their locations are mentioned in Table 2 and shown as blue and black filled triangles in Fig. 1. In this case three satellites PRN-3, PRN-16 and PRN-27 were locked at almost all stations at the time of earthquake and having the epicentral radial distance of IPP, within 1000 km (Fig. 3(i)a & b and Fig. 3(ii).a & b). In general, CIDs are observed clearly in all these stations (Figs. 3(i)c and 3(ii)c). Particularly, the PRN-27 was locked at seven GPS stations (PTH2, BDRI, GHUT, WIH2, LCK3, DELH, LHAZ). Station LCK3 located just south of Nepal in the Ganga Plain in India recorded an average VTEC of 85.4 ± 1.1 TECU, which is highest amongst all other six stations; while, station LHAZ situated at Northeast and far from the epicentre recorded the lowest of 65.4 ± 3.1 TECU. The regional trend in the VTEC of all stations have been removed through band pass filtering and the filtered VTEC anomalies are shown in Figs. 3(i)d and 3(ii)d. In general, the first

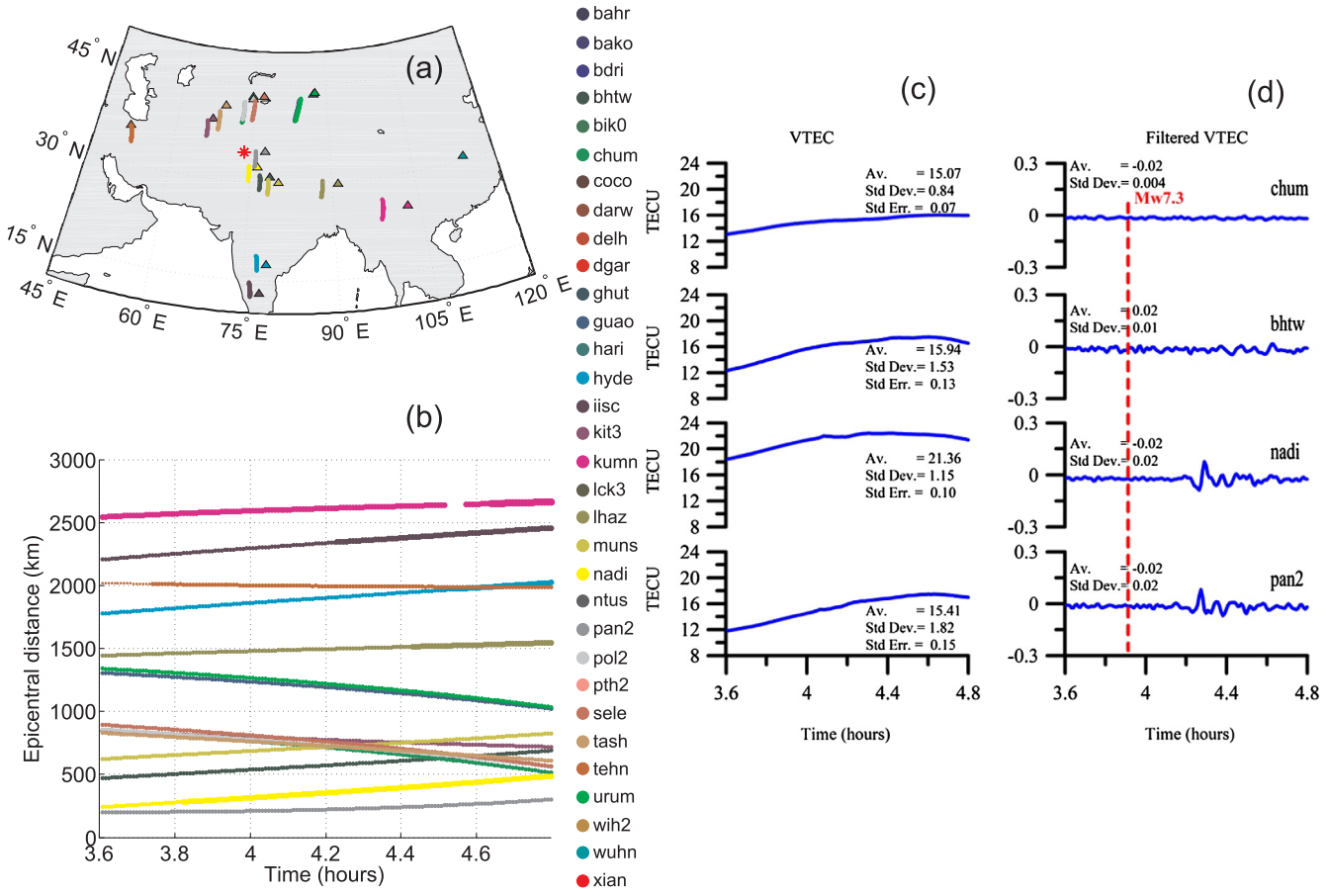

Fig. 4(i). . For locked satellite PRN-20 for the Kashmir 2005 earthquake: - (a) IPP plots at stations given in Table 3. (b) Epicentral distances of Ionospheric Piercing Point (IPPs) Vs time plots at stations given in Table 3. (c) Estimated Co-seismic ionospheric VTEC at each stations. (d) Band pass filtered Co-seismic ionospheric VTEC anomalies at each station.

VTEC anomaly in PRN-27 was detected at 06:32:29 UTC which was ~21 min after the earthquake occurrence. These disturbances were continued till 06:55:22 UTC and had a duration of 22.88 min. The corresponding VTEC anomaly amplitude variation for all stations is between −0.404 and 0.304 TECU (± 0.1); but at station LHAZ, comparatively small variation in VTEC anomaly is observed for PRN-27 (Fig. 3(i)d). However, for PRN-3 the first VTEC anomaly was observed at 06:29:58 UTC, which was 18.55 min after the occurrence of earthquake and it continued for a duration of 29.33 min, i.e. till 06:59:18 UTC (Fig. 3(ii)c). Since PRN-3 was available only at the far eastern side of the epicentre and also close to the station at LHAZ, hence the VTEC anomaly variation in LHAZ is quite sharp and varies from −0.635 to 0.700 TECU (± 0.01), which reflects a clear co-seismic spike (Fig. 3(ii) d). We deduce that the seismic signals associated with the Nepal earthquake could reach the ionosphere after 21.15 min from the time of earthquake occurrence. The duration of such a disturbance was observed around 22.78 min with the amplitude range of −0.442 to 0.370 (± 0.1) TECU.Fig. 3(ii).

(ii) The Mw 7.6 Kashmir earthquake on 8th October 2005

The Kashmir earthquake of 8th October 2005 was a Major Magnitude event of Mw 7.6 and had occurred in the Indus Kohistan Seismic Zone in the Northwestern Himalaya (Rao et al., 2006). The earthquake occurred along a tectonic boundary characterized by high seismic activity. The epicentre was located at 34.493°N, 73.629°E in the Kishanganga Valley about 10 km in the east of Balakot and 19 km in the northeast of Muzaffarabad in Pakistan. The Kishanganga valley lies in the Frontal Himalayan belt and bounded by the Main Boundary thrust and the Jhelum fault. The focal mechanisms from Harvard and US Geological Survey show that the earthquake was predominantly of a thrust type (Fig. 1). The large ground upheaval along Muzaffarabad and Tanda faults suggests that these active faults are responsible for the destructive earthquake (Reddy and Prajapati, 2009).

In this case, we have used seventeen permanent GPS stations to study the ionospheric TEC perturbation (Table 3). Station locations are shown in Fig. 1 as red and black filled triangles. During the time of earthquake two satellites with PRN-20 and PRN-23 were locked at all GPS sites (Figs. 4(i)a and 4(ii)a). Among the seventeen sites, only two sites at NADI and PAN2 are at a radial epicentral distances of their IPPs less than 1000 km, while the remaining stations having their epicentral distances greater than 1000 km (Figs. 4(i)b and 4(ii)b), hence significant CISs are not observed at other stations. Both NADI and PAN2 stations are located around 350 km towards southeast from the epicentre. The VTEC for PRN-20 and PRN-23 are shown in Figs. 4(i)c and 4(ii)c respectively. Average VTEC observed at NADI and PAN2 stations are 21.36 ± 1.15 TECU and 15.41 ± 1.82 TECU. In comparison with the Nepal earthquake the mean VTEC magnitudes in this case is relatively less. The filtered VTEC anomalies for both PRN's are given in Figs. 4(i)d and 4(ii)d. It is evident that significant anomalies are observed in PRN-20 and PRN-23 at PAN2 and NADI stations. For the case of PRN-23 (Fig. 4(ii)d), CIDs are detected only after 19.95 min of the earthquake occurrence and lasted for a duration of 18.1 min (04:10:37–04:28:43 UTC) with the amplitude variation from −0.228 to 0.368 (± 0.06) TECU; while for the case of PRN-20 (Fig. 4(i)d) it was observed 24 min later the earthquake and continued for 13 min (04:14:40–04:27:44 UTC) with relatively less amplitude variation from 0.066 to 0.081 (± 0.02) TECU. In general, the seismic signal generated

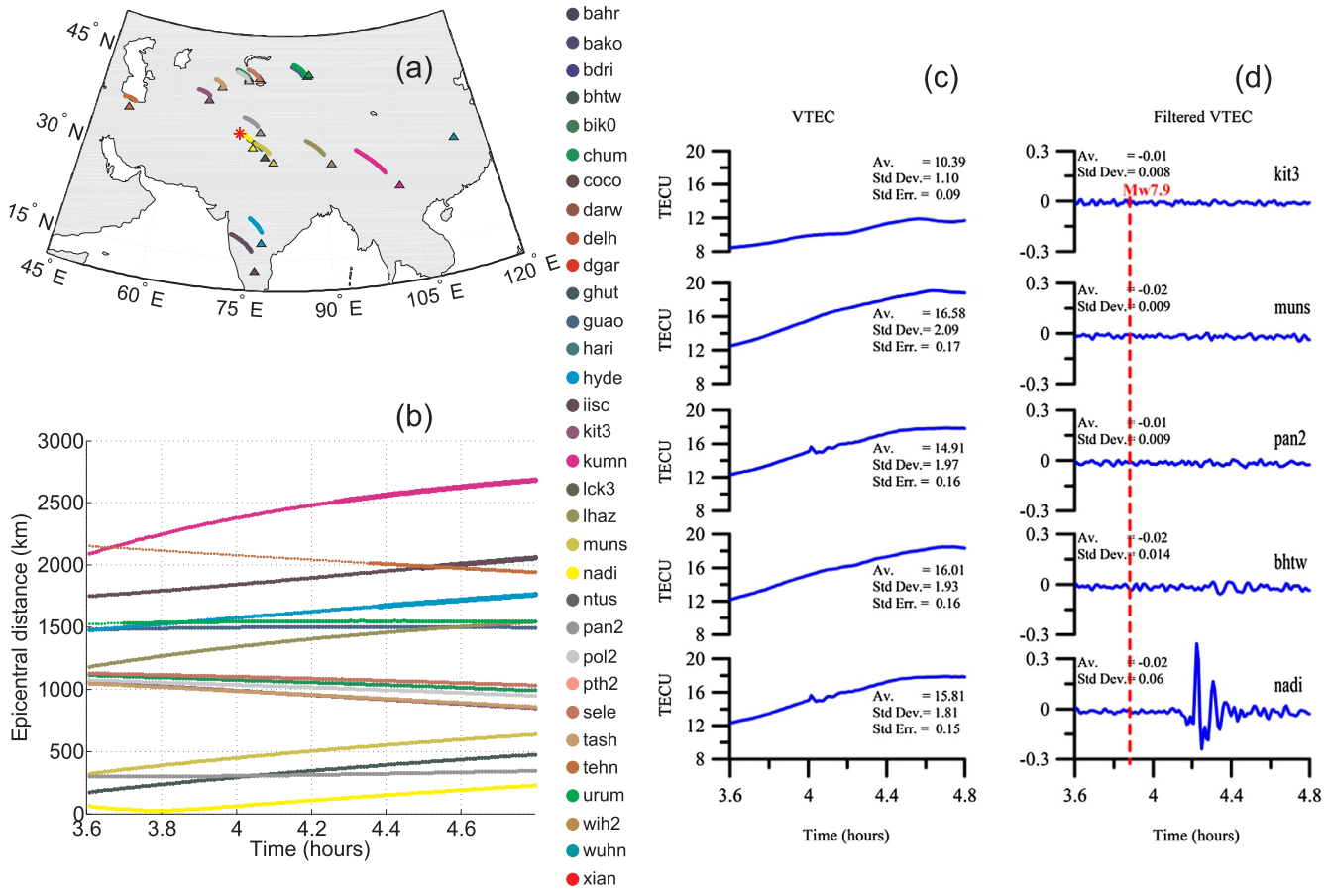

Fig. 4(ii). . For locked satellite PRN-23 for the Kashmir 2005 earthquake: - (a) IPP plots at stations given in Table 3. (b) Epicentral distances of Ionospheric Piercing Point (IPPs) Vs time plots at stations given in Table 3. (c) Estimated Co-seismic ionospheric VTEC at each stations. (d) Band pass filtered Co-seismic ionospheric VTEC anomalies at each station.

due to the Kashmir earthquake produces ionospheric VTEC anomaly after 23 min of earthquake occurrence and the disturbances continued for a duration of 14 min. although overall mean VTEC amplitude variation is from 15.41 ± 1.82 TECU to 21.36 ± 1.15 TECU.Fig. 4(ii)

(iii) The Mw 8.6, 28th March 2005 Nias–Simeulue earthquake (Sumatra earthquake, 2005)

The Nias-Simeulue earthquake was a Great earthquake occurred on 28th March 2005 at 16:09:35.29 UTC with M_W 8.6 (Hsu et al., 2006), which struck at the southwest of the Banda Aceh in the northern Sumatra and generated a small Tsunami. The epicentre was located at 1.64°N and 96.98°E, which is about 200 km in the southeast direction of the epicentre of the December 26, 2004 Great Sumatra earthquake (3.30°N, 95.78°E). Both earthquakes occurred near the junction of the Indian, Australian and Burma plates. It is known that the Indian plate is subducting below the Burmese micro-plate (at roughly 60 mm/year) along the Indonesia-Sumatra Trench line stretching from Indonesia in the south to the Andaman Islands in the north. The earthquake caused the rupture of a portion of the Sunda mega thrust at the offshore of the northern Sumatra (Konca et al., 2007). The December 26, 2004 earthquake and its aftershocks ruptured approximately 1200 km of this fault line, along the northern Sunda Trench. It has been estimated that the March 28, 2005 Nias-Simeulue earthquake had ruptured only about 400 km fault line and thereby filling in the gap between the 1861 earthquake and the 2004 Sunda-Andaman Great earthquake. The maximum displacement of the sea floor that got uplifted was slightly greater than 3 m, while the maximum negative seafloor displacement or the subsidence was roughly 1 m. It has been noted that the earlier Great Sumatra event of December 26, 2004 Mw 9.1 had generated an initial upliftment of the sea floor by about 7 m, that followed by a subsequent subsidence of about 3.5 m.

GPS data from 12 stations as listed in Table 4 and also shown as orange and black filled triangles in Fig. 1 have been used to analyse CIDs related to the 2005 Sumatra earthquake. At the time of earthquake incidence, there were six satellites locked (Fig. 5a) at all stations considered in the analysis (Table 4). However, the epicentral distances (Fig. 5b) of their IPPs were more than 1000 km due to which significant anomalies are not observed from COCO and BAKO stations (Fig. 5c). The station at NTUS is less than 1000 km epicentral distance of IPP for PRN-3, hence significant mean VTEC anomaly of 14.86 ± 1.25 TECU are observed and the same is shown in Fig. 5c. Seismic signals generated due to this earthquake interacted with the ionosphere and produced VTEC disturbances or anomalies at 16:09:10 UTC, which was after 25.58 min of the earthquake occurrence. This CIDs were continued for a duration of 17.92 min i.e. till 16:53:05 UTC with their TEC values vary from −0.077 to 0.058 (± 0.02) TECU (Fig. 5d).

The late registering of CIDs in the ionospheric layers associated with 2005 Sumatra earthquake appears conspicuous in comparison with other Himalayan earthquakes, because of the contrasting displacement of the ocean floor; such that, an initial uplift of the ocean floor was followed by a 3.5 m subsidence. In fact, the 2015 Gorkha event was also produced an initial upliftment of the ground followed by a subsidence. But what makes the early registering of CIDs from the Continent-Continent collision Himalayan Gorkha event different from the Ocean-Island Arc Niyas-Simeulue or Sumatra event was the effect of energy transfer through the atmospheric layers rather than through the water layer. The transfer of seismic energy from the Tsunami genic zone to the

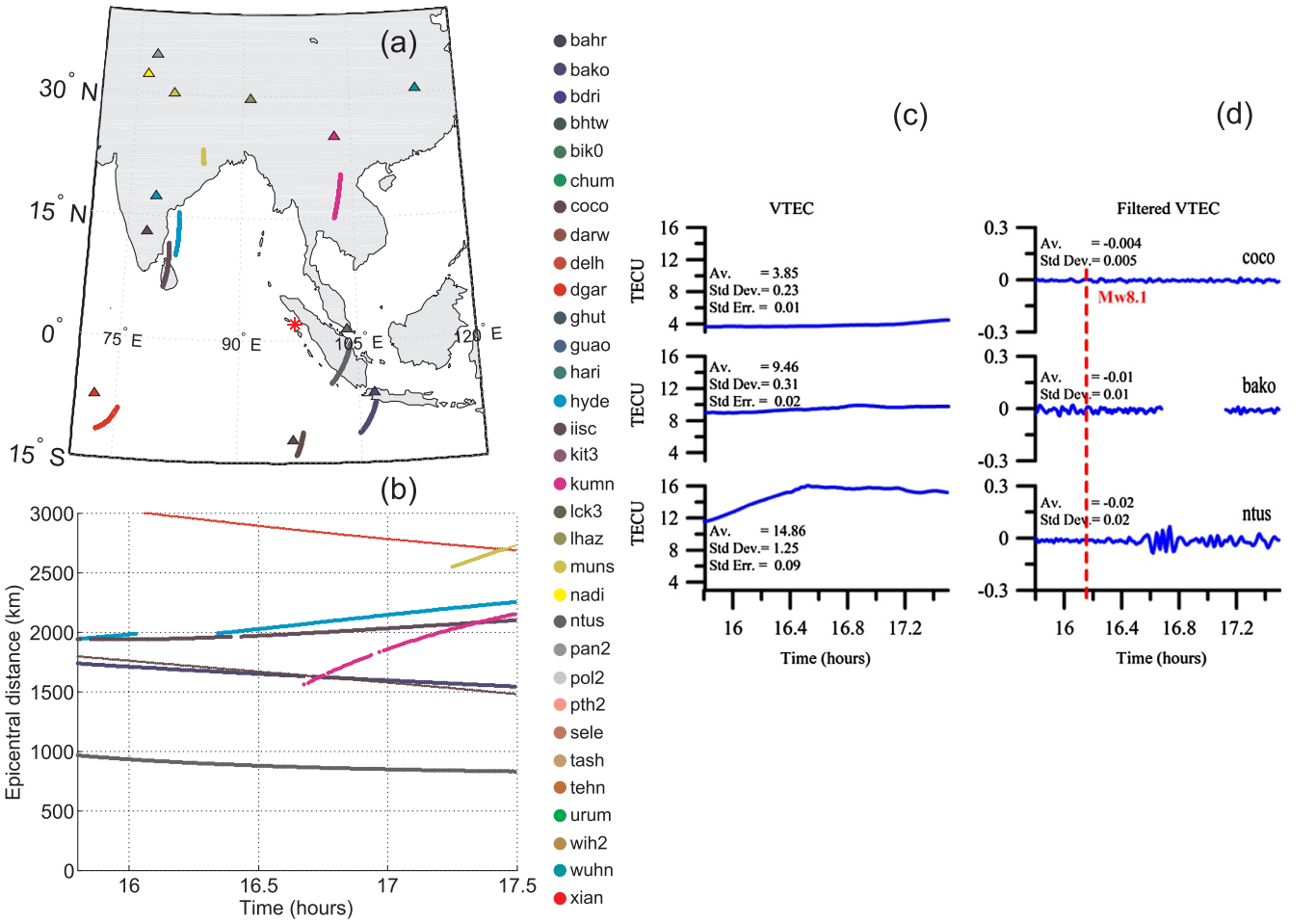

Fig. 5. . For locked satellite PRN-3 for the Sumatra 2005 earthquake: - (a) IPP plots at stations given in Table 4. (b) Epicentral distances of Ionospheric Piercing Point (IPPs) Vs time plots at stations given in Table 4. (c) Estimated Co-seismic ionospheric VTEC at each stations (d) Band pass filtered Co-seismic ionospheric VTEC anomalies at each station.

ionospheric layers was held by displacing almost 3.5–4 km thick water column. Here, the water layer acted as a low pass filter, which attenuated the propagation of high frequency seismic energy waves. Thus the effect of only the vertical displacement of the ocean floor at low frequency impulse got transferred to the over loading atmospheric layers and hence substantial delay is observed in registering the CIDs at the ionospheric layers. This is in fact, suggest the role of different coupling mechanism in transferring the seismic energy to the ionospheric layers from a Continental earthquake with respect to its Oceanic counterpart. The very critical part of the energy transfer from the earthquake rupture zone to the ionospheric height is the nature of lithospheric-ionospheric coupling mechanism. In this study, we were able to identify that there exist a different lithospheric-ionospheric coupling mechanism as far as registering of CIDs at the ionospheric height, that arise due to earthquakes from the Continental collision zone in Himalaya with respect to that from the Ocean-Island Arc collision zone.

5. Conclusions

We used continuously operating GPS data at different sites in the Himalaya and adjoining regions along with a few IGS stations data, to understand the co-seismic ionospheric disturbances that generated by a few Major and Great Magnitude Earthquakes occurred at the Continent-Continent and Ocean-Island Arc Plate boundary Margins of the Indian Tectonic plate. Two Major earthquakes in the Continent-Continent collision zone in the Himalaya; namely, the Gorkha Mw 7.9 earthquake of 25th April 2015 and the Mw 7.6 Kashmir Earthquake on 8th October 2005 show significant CIDs after the event in their respective PRN's. For the case of Central Himalayan Gorkha (Nepal) earthquake, anomalous vertical TEC are observed after 21.15 min of the earthquake and it was continued for a duration of 22.78 min from 06:32:34 hr to 06:55:21 hr with the amplitude range from −0.442 to 0.370 (± 0.1) TECU. The TEC perturbation was detected 23 min later for the case of Northwest Himalayan Kashmir earthquake and continued 14 min (04:13:39 hr to 04:27:44 hr) with an amplitude range from −0.120 to 0.177 (± 0.02) TECU. However, for the case of Ocean-Island Arc collision zone Sumatra earthquake; although it generated a small Tsunami, the first disturbance in the ionosphere was detected after 25.58 min of the earthquake occurrence and lasted about 17.92 min (16:35:10 hr–16:53:05 hr) with amplitude variation from −0.077 to 0.058 (± 0.02) TECU. Among the analyzed earthquakes, except those events mentioned in Table 1 could not produce any significant anomaly in ionospheric TEC, because (i) low magnitude and high focal depth (ii) very complex tectonic setting in the Himalaya and (iii) locked PRN over any stations having IPPs out of 1000 km. Through this study we have observed, firstly, the delay in registering of CIDs in the ionosphere that associated with the Tsunami genic Ocean-Island Arc Sumatra event; which highlight to the fact that the water column acts as a low pass filter in transferring the ocean bottom disturbances to the ionospheric layers. Secondly, the early registering of CIDs in the ionosphere by the Himalayan earthquakes with respect to the non-Himalayan earthquakes, suggest the operation of different lithospheric-ionospheric coupling mechanism in transferring the seismic energy originated from

the Continent-Continent and the Ocean-Island Arc collision zones. And finally the magnitude of vertical TEC for the case of Himalayan earthquakes is of the range of 15–90 TECU, while for the Ocean-Island originated earthquakes the maximum vertical TEC is not more than 15 TECU.

Acknowledgements

The authors are thankful to the Director, WIHG for the encouragement and support to carry out this work. Author John PP is thankful for the research fellowship from WIHG-IIRS/ISRO project. We also acknowledge the British Oceanography Data Centre (https://www.bodc.ac.uk/)- and USGS (https://lta.cr.usgs.gov/GTOPO30) for providing the GEBCO regional bathymetry-topography and Himalayan topography data respectively. The authors are thankful for the support of Mr. Saral Bagla, ISM Dhanbadh and Mr. C. P. Dabral, WIHG for their assistance.

References

Afraimovich, E.L., Perevalova, N.P., Plotnikov, A.V., Uralov, A.M., 2001. The shock-acoustic waves generated by the earthquakes. Ann. Geophys. 19 (4), 395–409.
Arora, B.R., Prajapati, S.K., Reddy, C.D., 2014. Geophysical constraints on the seismotectonics of the Sikkim Himalaya. Bull. Seismolog. Soci. America 104 (5), 2278–2287.
Artru, J., Farges, T., Lognonne, P., 2004. Acoustic waves generated from seismic surface waves: propagation properties determined from Doppler sounding observations and normal-mode modelling. Geophys. J. Int. 158, 1067–1077.
Astafyeva, E., Heki, K., 2009. Dependence of waveform of near-field coseismic ionospheric disturbances on focal mechanisms. Earth Planets Space 61, 939–943.
Astafyeva, E., Lognonné, P., Rolland, L., 2011. First ionosphere images for the seismic slip of the Tohoku-oki earthquake. Geophys. Res. Lett. 38, L22104.
Astafyeva, E., Shalimov, S., Olshanskaya, E., Lognonne, P., 2013. Ionospheric response to earthquakes of different magnitudes: larger quakes perturb the ionosphere stronger and longer. Geophys. Res. Lett. 40, 1675–1681.
Avouac, J.P., Meng, L., Wei, S., Wang, T., Ampuero, J.P., 2015. Lower edge of locked main Himalayan thrust unzipped by the 2015 Gorkha earthquake. Nat. Geosci. 8, 708–711.
Banerjee, P., Pollitz, F.F., Burgmann, R., 2005. The size and duration of the Sumatra-Andaman earthquake from far-field static offsets. Science 308, 1769–1772.
Bilham, R., Larson, K., Freymueller, J., 1997. GPS measurements of present-day convergence across the Nepal Himalaya. Nature 386, 61–64.
Bishop, R.L., Aponte, N., Earle, G.D., Sulzer, M., Larsen, M.F., Peng, G.S., 2006. Arecibo observations of ionospheric perturbations associated with the passage of Tropical Storm Odette. J. Geophys. Res. 111, A1132.
Cahyadi, M.N., Heki, K., 2013. Ionospheric disturbances of the 2007 Bengkulu and the 2005 Nias earthquakes, Sumatra, observed with a regional GPS network. J. Geophys. Res. Space Phys. 118, 1–11.
Cahyadi, M.N., Heki, K., 2015. Coseismic ionospheric disturbance of the large strike-slip earthquakes in North Sumatra in 2012: Mw dependence of the disturbance amplitudes. Geophys. J. Int. 200, 116–129.
Calais, E., Minster, J.B., 1996. GPS detection of ionospheric perturbations following a Space Shuttle ascent. Geophys. Res. Lett. 23, 1897–1900.
Davies, K., 1980. Recent progress in satellite radio beacon studies with particular emphasis on the ATS-6 radio beacon experiment. Space Sci. Rev. 25, 357–430.
Ding, F., Wan, W., Mao, T., Wang, M., Ning, B., Zhao, B., Xiong, B., 2014. Ionospheric response to the shock and acoustic waves excited by the launch of the Shenzhou 10 spacecraft. Geophys. Res. Lett. 41, 3351–3358.
Ducic, V., Artru, J., Lognonne, P., 2003. Ionospheric remote sensing of the Denali earthquake Rayleigh surface waves. Geophys. Res. Lett. 30 (18), 1951–1954.
Dziewonski, A.M., Chou, T.A., Woodhouse, J.H., 1981. Determination of earthquake source parameters from waveform data for studies of global and regional seismicity. J. Geophys. Res. 86, 2825–2852.
Ekström, G., Nettles, M., Dziewonski, A.M., 2012. The global CMT project 2004–2010: centroid-moment tensors for 13,017 earthquakes. Phys. Earth Planet. Inter. 200–201, 1–9.
Gaivoronskaya, T.V., Pulinets, S.A., 2002. Analysis of F2-layer variability in the areas of seismic activity. Preprint IZMIRAN No. 2 (1145) Moscow, 20 p.
Gansser, A., 1964. Geology of the Himalayas. Wiley-Interscience, New York, pp. 289.
Heki, K., 2011. Ionospheric electron enhancement preceding the 2011 Tohoku-Oki earthquake. Geophys. Res. Lett. 38, L17312.
Hocke, K., Pavelyev, A.G., 2001. General aspect of GPS data use for atmospheric science. Adv. Space Res. 27, 1313–1320.
Hofmann-Wellenhof, B., Lichtenegger, H., Collins, J., 2001. Global Positioning System: Theory and Practice. Springer, Berlin.
Hsu, Ya-Ju., Simons, M., Avouac, J,P., Galetzka, J., Sieh, K., Chlieh, M., Natawidjaja, D., Prawirodirdjo, L., Bock, Y., 2006. Frictional Afterslip Following the 2005 Nias-Simeulue Earthquake, Sumatra, Science, 312, 1921–1926.
Huang, Y.N., Kang, C., Chen, S.W., 1985. On the detection of acoustic gravity waves generated by typhoon by use of real time HF Doppler frequency shift sounding system. Radio Sci. 20, 897–906.
Kakinami, Y., Kamogawa, M., Tanioka, Y., Watanabe, S., Gusman, A.R., Liu, J.-Y., Watanabe, Y., Mogi, T., 2012. Tsunamigenic ionospheric hole. Geophys. Res. Lett. 39, L00G27.
Klobuchar, J.A., 1986. Ionospheric time-delay algorithm for single frequency GPS users. IEEE Trans. Aerosp. Electron. Syst. AES 23 (3), 325–331.
Konca, A.O., Hjorleifsdottir, V., Song, T.A., Avouac, J., Helmberger, D.V., Chen, J., Sieh, K., Briggs, R., Meltzner, A., 2007. Rupture kinematics of the 2005 Mw 8.6 Nias-Simeulue earthquake from the joint inversion of seismic and geodetic data. Bull. Seismol. Soci Am. 97, 1A, S307–S322.
Kumar, A., Sanoujam, M., Roy, L.S., Kosigyn, L., Singh, W.A.R., Pandey, A.P., 2016. M w6.7 earthquake of manipur, NE India: some insights. J. Geological Soc. India 88, 5–12.
Kumar, N., Paul, A., Mahajan, A.K., Yadav, D.K., Bora, C., 2012a. Mw 5.0 Kharsali, Garhwal Himalaya earthquake of July 23, 2007: source characterization and tectonic implication. Curr. Sci. 102, 1674–1682.
Kumar, S., Priyadarshi, S., Gopi Krishna, S., Singh, A.K., 2012b. GPS-TEC variations during low solar activity period (2007–2009) at Indian low latitude stations. Astrophys Space Sci. 339, 165–178. http://dx.doi.org/10.1007/s10509-011-0973-6.
Liperovsky, V.A., Pokhotelov, O.A., Shalimov, S.A., 1992. Ionospheric Precursors of the Earthquakes. Nauka, Moscow, 304 p (in Russian).
Liu, J.Y., Tsai, Y.B., Chen, S.W., Lee, C.P., Chen, Y.C., Yen, H.Y., Chang, W.Y., Liu, C., 2006. Giant ionospheric disturbances excited by the M9.3 Sumatra earthquake of 26 December 2004. Geophys. Res. Lett. 33 (L02103).
Liu, J.-Y., Chen, C.-H., Lin, C.-H., Tsai, H.-F., Chen, C.-H., Kamogawa, M., 2011. Ionospheric disturbances triggered by the 11 March 2011 M9.0 Tohoku earthquake. J. Geophys. Res. 116 (A06319).
Occhipinti, G., Dorey, P., Farges, T., Lognonné, P., 2010. Nostradamus: the radar that wanted to be a seismometer. Geophys. Res. Lett. 37, L18104.
Ogawa, T., Nishitani, N., Tsugawa, T., Shiokawa, K., 2012. Giant ionospheric disturbances observed with the SuperDARN Hokkaido HF radar and GPS network after the 2011 Tohoku earthquake. Earth Planets Space 64, 1295–1307.
Otsuka, Y., Kotake, N., Tsugawa, T., Shiokawa, K., Ogawa, T., Saito, S., Kawamura, M., Maruyama, T., Hemmakorn, N., Komolmis, T., 2006. GPS detection of total electron content variations over Indonesia and Thailand following the 26 December 2004 earthquake. Earth Planets Space 58, 159–165.
Ozeki, M., Heki, K., 2010. Ionospheric holes made by ballistic missiles from North Korea detected with a Japanese dense GPS array. J. Geophys. Res. 115, A09314.
Parrot, M., Achache, J., Berthelier, J.J., Blanc, E., Deschamps, A., Lefeuvre, F., Menvielle, M., Plantet, J.L., Tarits, P., Villain, J.P., 1993. High frequency seismo-electromagnetic effects. Phys. Earth Planet. Inter. 77, 65–83.
Perevalova, N.P., Sankov, V.A., Astafyeva, E.I., Zhupityaeva, S., 2014. Threshold magnitude for ionospheric TEC response to earthquakes. J. Atmos. Terr. Phys. 1–8, 77–90.
Pollitz, F.F., Banerjee, P., Burgman, R., Hashimoto, M., Choosakul, N., 2006. Stress changes along the Sunda trench following the 26 december 2004 Sumatra-Andaman and 28 march 2005 Nias earthquakes. J. Geophy. Res. Lett. 33, L06309.
Pulinets, S.A., Leyva Contreras, A., Bisiacchi, G., Ciraolo, L., Singh, R., 2003. Ionospheric and thermal precursors of Colima earthquake of 22 January 2003. Ann. Meeting Mexican Geophys. Union GEOS 23, 170.
Pulinets, S., 2004. Ionospheric precursors of earthquakes; recent advances in theory and practical applications. Terr. Atmos. Oceanic Sci. 15, 413–435.
Rama Rao, P.V.S., Krishna, S. Gopi, Niranjan, K., Prasad, D.S.V.V.D., 2006. Temporal and spatial variations in TEC using simultaneous measurements from the Indian GPS network of receivers during the low solar activity period of 2004–2005. Ann. Geophys. 24, 3279–3292.
Rao, N.P., Kumar, P., Tsukuda, T., Ramesh, D.S., 2006. The devastating Muzaffarabad earthquake of 8 October 2005: new insights into Himalayan seismicity and tectonics. Gondwana Res. 9, 365–378.
Reddy, C.D., Prajapati, S.K., 2009. GPS measurements of postseismic deformation due to October 8, 2005 Kashmir earthquake. J. Seismol. 13, 415–420.
Reddy, C.D., Seemala, G.K., 2015. Two-mode ionospheric response and Rayleigh wave group velocity distribution reckoned from GPS measurement following Mw 7.8 Nepal earthquake on 25 April 2015. J. Geophys. Res. Space Phys. 120, 7049–7059.
Reddy, C.D., 2016. Seismo-ionospheric anomalies and implications from recent GNSS observations in India and South-East Asia. J. Geodesy Geodynamics 7 (1), 11–18.
Rolland, L.M., Lognonné, P., Munekane, H., 2011a. Detection and modeling of Rayleigh wave induced patterns in the ionosphere. J. Geophys. Res. 116, A05320.
Rolland, L.M., Lognonne, P., Astafyeva, E., Kherani, E.A., Kobayashi, N., Mann, M., Munekane, H., 2011b. The resonant response of the ionosphere imaged after the 2011 off the Pacific coast of Tohoku earthquake. Earth Planets Space 63, 853–857.
Row, R.V., 1967. Acoustic-gravity waves in the upper atmosphere due to a nuclear detonation and an earthquake. J. Geophys. Res. 72, 1599–1610.
Ryu, K., Lee, E., Chae, J.S., Parrot, M., Pulinets, S., 2014. Seismo-ionospheric coupling appearing as equatorial electron density enhancements observed via DEMETER electron density measurements. J. Geophys. Res. Space Phys. 119, 8524–8542.
Saito, A., Tsugawa, T., Otsuka, Y., Nishioka, M., Iyemori, T., Matsumura, M., Saito, S., Chen, C.H., Goi, Y., Choosakul, N., 2011. Acoustic resonance and plasma depletion detected by GPS total electron content observation after the 2011 off the Pacific coast of Tohoku earthquake. Earth Planets Space 63, 863–867.
Seemala, G.K., Valladares, C.E., 2011. Statistics of total electron content depletions observed over the South American continent for the year 2008. Radio Sci. 46 (RS5019).
Sunil, A.A., Bagiya, M.S., Reddy, C.D., Kumar, M., Ramesh, D.D., 2015. Post-seismic ionospheric response to the 11 April 2012 East Indian Ocean doublet earthquake. Earth Planets Space 67 (37), 1–12.
Trigunait, A., Parrot, M., Pulinets, S., Li, F., 2004. Variations of the ionospheric electron density during the Bhuj seismic event. Ann. Geophys. 22, 4123–4131.
Tsugawa, T., Saito, A., Otsuka, Y., Nishioka, M., Maruyama, T., Kato, H., Nagatsuma, T., Murata, K.T., 2011. Ionospheric disturbances detected by GPS total electron content observation after the 2011 off the Pacific coast of Tohoku earthquake. Earth Planets Space 63, 875–879.